# Ductile Crack Extension in Compact Specimens at Limit Load

JUN MING HU*, JIANGUO CHENG**,
PEDRO ALBRECHT*** and JAMES JOYCE†

*Graduate Research Assistant, Department of Civil Engineering, University of Maryland, College Park, Maryland, USA
**Associate Professor, Department of Mechanical Engineering, Nanjing Institute of Chemical Technology, Nanjing, PRC
***Professor, Department of Civil Engineering, University of Maryland, College Park, Maryland, USA
†Professor, Department of Mechanical Engineering, US Naval Academy, Annapolis, Maryland, USA

## INTRODUCTION

The deformation field of a cracked specimen fabricated from a highly ductile material is affected by the geometry of the specimen far from the crack tip and by the details of loading. In this case crack extension is defined by plastic rotation of specimen or structure subelements, i.e. specimen halves, and occurs strictly at limit load; it cannot be predicted with single-parameter singularity solutions. Definition of the boundary between elastic-plastic behavior in which singularity parameters might control crack extension and plastic behavior where structure deformation defines crack extension is an important problem in ductile fracture mechanics.

In a first step towards such a distinction, limit load equations reported in the literature for compact specimens [C(T)] are reviewed, modified as needed, and then used to predict the measured load versus crack extension behavior of compact specimens of different size, initial crack length, and type of steel.

## LITERATURE REVIEW

The previous limit load solutions for compact specimens can be classified into four types in accordance with the assumed slip field or stress distribution at limit load. These are: (1) circular-linear slip line; (2) circular slip line; (3) symmetrical slip line; and (4) rectangular yield stress distribution.

The solutions that are based on a circular-linear slip line originated from the work by Green (1953), and Green and Hundy (1956) who derived the limit moment for a plate with a wedge-like or circular notch subjected to pure bending. The circular-linear slip line gives a constraint factor of 1.26 when the notch angle approaches zero, a case resembling that of an edge crack in a plate under pure bending. The limit moment was derived from the equations of equilibrium between the external and internal stress resultants, giving a lower-bound solution for the limit moment. Subsequently, various investigators applied the circular-linear slip line solution to the following combinations of geometry and loading condition:

three-point-bend specimen under pure bending of the uncracked ligament (Landes and Begley, 1972; and Bucci et al., 1972); single-edge-notched and double-cantilever-bend specimens subjected to tension and bending (Ewing and Richards, 1974); and compact tension specimen subjected to tension and bending (Royer et al., 1979; Shiratori and Miyoshi, 1981; and Kumar and Shih, 1980).

In the second type of solution, Rice (1972) assumed a circular slip line in an edge-cracked plate subjected to tension and bending. The limit load was obtained by the mechanism method in which the external work done by a rotation of the plastic hinge was equated to the internal work done by the shear stresses along the slip line, giving an upper-bound solution. Because the equations could not be solved in closed form, Rice conservatively approximated all solutions for combined tension and bending with an elliptical curve. McMeeking (1984) applied Rice's solution to the compact tension specimen.

In the third type of solution, Schmitt and Keim (1980) assumed a symmetrical, circular slip line with slope of 45 deg at the crack tip and -45 deg at the back face and calculated the limit load with the finite element method.

Finally, the fourth type of solution assumed a distribution of the normal stresses along the uncracked ligament. Two such solutions are commonly known. In one, Merkle and Corten (1974) calculated the limit load based on the equilibrium between the external axial force and moment and the assumed rectangular distribution of yield stress in tension and compression acting on the uncracked ligament. The value of the limit load was later multiplied by a constraint factor. In the other, ASTM Specification E813 lists an approximate value of the limit load for compact specimens that was based on a linear-elastic stress distribution for combined tension and bending, with a maximum stress of two times the yield stress. The factor of two is about equal to Green's constraint factor for pure bending, 1.26, times the ratio of plastic moment to yield moment of a rectangular section, 1.5.

In the present study the effect of an axial force is added to Green's (1953) solution for pure bending and a numerical, closed-form limit load equation is fitted to Rice's (1972) solution.

## MODIFIED GREEN SOLUTION

Green's solution can be modified to include both the effect of the axial force, P, and moment, M, acting on the uncracked ligament. Fig. 1(a) shows the slip line in the upper half of a compact specimen, consisting of a circular segment of included angle $(\alpha+\beta)$ and a linear segment that intersects the back face at a 45-deg angle. The lower slip line, not shown in the figure, is symmetrical with respect to the x-axis. According to Green's solution for a wedge-like notch with a wedge angle approaching zero, the angles $\alpha$ and $\beta$ of the circular segment must satisfy the condition

$$\tan(\alpha+\beta) = \frac{(\alpha+\beta)}{1 - (\alpha+\beta)} \tag{1}$$

giving $\alpha + \beta = 117.02$ deg.

For any point on the slip line, the shear stress is equal to the yield



(maximum) shear stress, k. Therefore, according to Mohr's circle, the stress normal to the slip line is equal to the mean stress, $\sigma_m = 0.5\,(\sigma_x + \sigma_y)$, [Fig. 1(b)]. These stresses must satisfy the property of the slip line

$$\sigma_m - 2k\theta = \text{const.} \tag{2}$$

where $\theta$ = angle of slip line with x-axis. Rotating an element on the slip line clockwise by an angle $\theta$ gives the stresses on the x- and y-faces of the element in accordance with Mohr's circle [Fig. 1(c)].

$$\sigma_x = \sigma_m - k \sin 2\theta \tag{3}$$

$$\sigma_y = \sigma_m + k \sin 2\theta \tag{4}$$

$$\sigma_{xy} = k \cos 2\theta \tag{5}$$

The constant and mean stress in Eq. 2 are obtained from the state of stress at point C where the slip line intersects the free surface. At this point the angle is assumed to be $\theta = -45$ deg (Green, 1953). Furthermore, because $\sigma_x = 0$ at the free surface, it follows from Eqs. 3 and 4 that $\sigma_y = -2k$ at point C [Fig. 1(d)]. Substituting these values of $\theta$ and $\sigma_y$ into Eqs. 2 and 4 gives the constant

$$\text{const.} = \left(\frac{\pi}{2} - 1\right) k \tag{6}$$

and the mean stress

$$\sigma_m = \left(\frac{\pi}{2} - 1\right) k + 2k\theta \tag{7}$$

needed to calculate with Eqs. 3 to 5 the stresses $\sigma_x$, $\sigma_y$, and $\tau_{xy}$ at any point on the slip line. From the geometry of the slip line it follows that $\beta = 45$ deg and hence $\alpha = 72.02$ deg.

It can be shown that the condition of horizontal equilibrium, $\Sigma F_x = 0$, is satisfied for the free-body diagram obtained by cutting the compact specimen along the upper slip line [Fig. 1(b)]. Similarly, the equilibrium of the vertical forces at limit load, $\Sigma F_y = 0$, gives

$$-P_L + \int_{-\beta}^{\alpha} \left[\left(\frac{\pi}{2} - 1\right) + 2\theta\right) k \cos\theta + k \sin\theta\right] B\, R\, d\theta$$

$$- \left[k \sin\frac{\pi}{4} + k \cos\frac{\pi}{4}\right] B \left[b - R(\sin\alpha + \sin\beta)\right] \left(\sin\frac{\pi}{4}\right)^{-1} = 0 \tag{8}$$

where b = uncracked ligament, B = specimen thickness, and R = radius of circular slip line. Solving Eq. 8 leads to

$$P_L = (5.144\, R - 2b)\, k\, B \tag{9}$$

Finally, the equilibrium of all moments about the center of rotation, $\Sigma M_O = 0$, gives

$$P_L(a + R \sin\alpha) - \int_{-\beta}^{\alpha} kB\, R^2 d\theta - kB\,[b - R(\sin\alpha + \sin\beta)]\,\sqrt{2}\,R$$

$$- kB\,[b - R(\sin\alpha + \sin\beta)]^2 = 0 \qquad (10)$$

where a = crack size. Assuming $k = \sigma_{ys}/\sqrt{3}$ in accordance with the von Mises yield criterion and solving Eqs. 9 and 10 for the two unknowns R and $P_L$ gives the radius of the circular segment of the slip line

$$R = \sqrt{(1.052\,a)^2 + 0.409(2ab + b^2)} - 1.052\,a \qquad (11)$$

and the limit load

$$P_L = \frac{2}{\sqrt{3}}\, WB\, \sigma_{ys}\, (2.572\,\frac{R}{b} - 1)(1 - \frac{a}{W}) \qquad (12)$$

where W = specimen width.

## FITTED RICE SOLUTION

Rice assumed a circular slip line emanating from the tip of an edge crack of size, a, in a plate of width, W, subjected to axial force and bending (Fig. 2). A virtual rotation of the plastic hinge mechanism gives the following upper bound inequality of the external and internal work

$$M_L + P_L\,(\frac{W-a}{2} - R\sin\beta) \leq kR^2\,(\alpha+\beta) \qquad (13)$$

where $P_L$ and $M_L$ = limit load and moment acting at mid-length of the uncracked ligament, b; R = radius of slip curve; and $\alpha$ and $\beta$ = included angles. Eq. 13 contains the five unknowns $P_L$, $M_L$, R, $\alpha$, and $\beta$. The four additional equations needed for the calculation of the limit load are obtained from the requirement that the internal work (right side of Eq. 13) be a minimum

$$\frac{\partial}{\partial\alpha}\,[kR^2\,(\alpha+\beta)] = 0 \qquad (14)$$

$$\frac{\partial}{\partial\beta}\,[kR^2\,(\alpha+\beta)] = 0$$

as well as the geometric relationship

$$W - a = R\sin\alpha + R\sin\beta \qquad (15)$$

and the relationship between the load and moment

$$M_L = P_L\,\frac{W+a}{2} \qquad (16)$$



According to Rice, Eqs. 14 to 15 lead to the following expression between the angles

$$2(\alpha+\beta) = \tan\alpha + \tan\beta \qquad (17)$$

For each set of angles $\alpha$ and $\beta$ satisfying Eq. 17, the upper bound inequality (Eq. 13) gives a straight line in a plot of P versus M. All such straight lines envelope the yield surface, which Rice conservatively approximated with an elliptical curve.

The writers numerically solved the above equations for the values of $P_L$ and $M_L$ corresponding to crack sizes varying from a/W = 0.5 to 1.0, and fitted the numerical results with the following equation for the limit load based on the von Mises criterion:

$$P_L = [0.711 - 1.789\,\frac{a}{W} + 1.453\,(\frac{a}{W})^2 - 0.376\,(\frac{a}{W})^3]\, WB\,\sigma_{ys} \qquad (18)$$

This more accurate fit gives a higher limit load than Rice's conservative elliptical fit, by 4 percent at a/W = 0.5 to 11 percent at a/W = 1.0.

## COMPARISON OF PRESENT LIMIT LOAD SOLUTIONS

The two limit load equations developed in the present study were compared in Figs. 3, 4, and 5. As would be expected, the upper-bound fitted Rice solution gives a higher limit load (Eq. 18) than the lower-bound modified Green solution (Eq. 12). Because the two bounds differ by at most three percent, it can be assumed that the limit load Eqs. 12 and 18 are accurate within $\pm$ 3.0 percent.

In comparison, Green's previous solution for pure bending overestimates and Rice's previous fit underestimates the limit load of a compact specimen. As a result, Rice's previous solution actually falls below Green's previous solution, contrary to what would be expected from the static and kinematic theorems. The present solutions correctly bracket the limit load.

## COMPARISON WITH EXPERIMENTAL RESULTS

The two limit load Eqs. 12 and 18 were compared with data from single-specimen, unloading compliance tests of compact specimens to determine whether the measured load versus crack extension behavior could be predicted for different initial crack sizes, specimen sizes, and types of metal. Table 1 lists the measured tensile properties for each material and the test temperature. The tests were performed using an unloading compliance method in accordance with ASTM Specification E1152.

The predicted curves were based on the net specimen width, $B = B_n$; the flow stress, $\sigma_o = 0.5\,(\sigma_{ys} + \sigma_u)$, where $\sigma_{ys}$ and $\sigma_u$ are the measured yield and tensile strengths listed in Table 1; and the von Mises yield criterion, $k = \sigma_o/\sqrt{3}$. Each data point in Figs. 3, 4, and 5 corresponds to a point on the measured load-displacement curve at which the specimen was partially unloaded to determine the crack extension from the compliance.

Initial Crack Size: Fig. 3 shows the data for four 1T-C(T) specimens fabricated from ASTM A533B quenched and tempered pressure vessel steel that was alloyed with manganese, molybdenum, and nickel. The specimens were not side grooved and had initial crack sizes of $a_i/W$ = 0.55, 0.63, 0.72, and 0.81. The tests were terminated after about six-percent crack extension, $\Delta a = 0.06\ a_i$. The test temperature was 150°C. In each test the load rose to the maximum measured value, the crack extended, and the measured curves gradually aligned themselves with the two predicted limit load curves.

Specimen Size: Fig. 4 shows the data for two compact specimens, one of 1/2T (12.5 mm) and the other of 1T (25 mm) size. Both were side grooved 20 percent, giving a net thickness of $B_n$ = 10 and 20 mm, respectively, in the plane of the crack. The specimens were fabricated from a quenched and tempered 3% $N_i$ alloy steel. The tests were started at an initial crack size of $a_i/W$ = 0.60 and terminated after the crack had extended up to $\Delta a = 0.46\ a_i$. The specimens were tested at room temperature. The results were plotted in terms of the limit load normalized by the flow stress, net thickness, and specimen size. Both measured curves agreed very well with the predicted limit loads over the full range of crack extension.

Type of Metal: In the third comparison, Fig. 5 shows the data for four 1T-C(T) specimens fabricated from A533B steel; 3% Ni steel; ASTM A710, a low-carbon, age-hardening, nickel-copper-chromium-molybdenum-columbium alloy steel; and CS-19 aluminum, a aluminum-magnesium alloy with high yield and tensile strengths. The A533B steel specimen was tested at 150° C, the other three at room temperature. The specimens were 20-percent side grooved and had initial crack sizes varying from 0.61 to 0.75 a/W. The tests were carried out to crack extensions greatly exceeding the ten percent of a/W permitted in the ASTM E1152 J-R curve test method. As with the previous data, the measured curves for 3% Ni steel and CS-19 aluminum agreed very well with the predicted limit loads, whereas those for A533B steel and A710 steel were well above the predicted limit loads.

The relative positions of these four materials in Fig. 5 correspond directly to the relative toughness as defined by the measured value of $J_{1C}$ (ASTM E813) listed for each material in Table 1. The high-toughness alloy specimens showed significantly more specimen deformation, allowing strain hardening to increase the observed limit load. Also apparent on the A710 steel specimens was a lateral expansion of the specimen and closing of the side groves at the back face which could have contributed to the observed elevation in limit load as the test progressed.

## CONCLUSIONS

In the present limit load analysis of the compact specimen, Green's (1953) lower-bound solution for pure bending was modified to account for the additional effect of axial force. For the case of a sharp crack geometry, a closed-form solution was obtained for the limit load and the radius of rotation of the deforming compact geometry. The previous approximate upper-bound solution of Rice (1972) was evaluated by fitting a polynomial function to the transcendental equation, giving a more accurate solution especially for ratios of axial force and bending typical of the compact specimen. The upper- and lower-bound results are consistent with each other within 3 percent, from a/W = 0.5 to 1.0.



Assuming the von Mises yield criterion holds and the flow stress is equal to the mean of the yield and tensile strengths, the calculated limit loads corresponded well with the experimentally measured load versus crack extension behavior of compact specimens. These results were very consistent despite the wide range of initial crack size, $a_i/W$ = 0.55 to 0.81; 1/2T and 1T-C(T); and fracture toughness, $J_{1c}$ = 25 kJ/m$^2$ for the aluminum and $J_{1c}$ = 183 to 435 kJ/m$^2$ for the steel specimens.

The presence or absence of singularity controlled crack extension could not be determined. Using the improved understanding of the solution for the slip line field, the writers are seeking suitable criteria for distinguishing the crack extension controlled by a singularity parameter from that defined by deformation at limit load.

## REFERENCES


Green, A.P.(1953). "The plastic yielding of notched bars due to bending," Journal of Mechanics and Applied Mathematics, 6, Part 2, 223-239.

Green, A.P. and Hundy, B.B. (1956). "Initial plastic yielding in notch bend tests," Journal of the Mechanics and Physics of Solids, 4, 128-145.

Landes, J.D. and Begley, J.A. (1972). "The effect of specimen geometry on $J_{1c}$," ASTM STP 514, Part 2, 24-39.

Bucci, R.J., Paris, P.C., Landes, J.D., and Rice, J.R. (1972). "J-integral estimation procedures," ASTM STP 514, Part 2, 40-69.

Ewing, D.J.F. and Richards, C.E. (1974). "The yield-point loads of singly-notched pin-loaded tensile strips," Journal of the Mechanics and Physics of Solids, 22, 27-36.

Royer, J., Tissot, J.M., Pelissier-Tanon, A., Le Poac, and Miannay, D. (1979). "J-integral dederminations and analysis for small test specimens and their usefulness for estimating fracture toughness," Elastic-Plastic Fracture, ASTM STP 668, 334-357.

Shiratori, M. and Miyoshi, T. (1981). "Evaluation of J-integral and COD for compact tension specimen," Fracture Mechanics of Ductile and Tough Materials and Its Applications to Energy Related Structures, Proceedings of the USA-Japan Joint Seminar, Japan, 89-97.

Kumar, V. and Shih, C.F. (1980). "Fully plastic crack solution, estimation scheme, and stability analyses for the compact specimen," ASTM STP 700, 406-436.

Rice, J.R. (1972). "The line spring model for surface flaws," In Surface Crack: Physical Problems and Computational Solutions, ASME Winter Meeting, 171-185.

McMeeking, R.M. (1984). "Estimates of the J-integral for elastic-plastic specimens in large scale yielding," Journal of Engineering Materials and Technology, 106, 278-284.

Schmitt, W. and Keim, E. (1980). "Numerical aspects of elastic-plastic fracture mechanics including 3D-applications," Advances in Elasto-Plastic Fracture Mechanics, Edited by L.H. Larsson, CEC Joint Research Centre, Ispra Establishment, Italy.

Merkle, J.G. and Corten, H.T. (1974). "A J-integral analysis for the compact specimen, considering axial force as well as bending effects," Journal of Pressure Vessel Technology, ASME, 286-292.

Table 1 Properties of Materials

| Material | Yield Strength $\sigma_{ys}$ (MPa) | Ultimate Strength $\sigma_u$ (MPa) | Flow Stress $\sigma_o$ (Mpa) | Total Elongation $\delta$ (%) | Fracture Toughness $J_{1c}$ ($kJ/m^2$) | Test Temperature T (°C) |
|---|---|---|---|---|---|---|
| A710 | 517 | 605 | 561 | 31 | 435 | RT |
| A533B | 448 | 621 | 534 | 19 | 240 | 150 |
| 3% Ni steel | 614 | 731 | 672 | 23 | 183 | RT |
| CS-19 | 251 | 408 | 329 | 24 | 25 | RT |

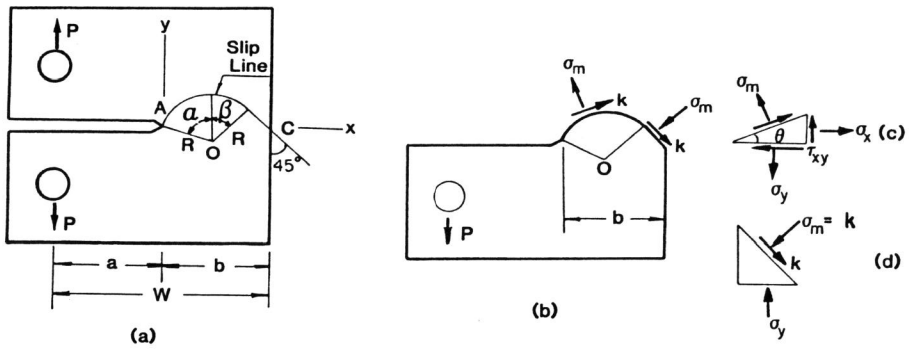


Fig. 1. Circular - Linear Slip Line



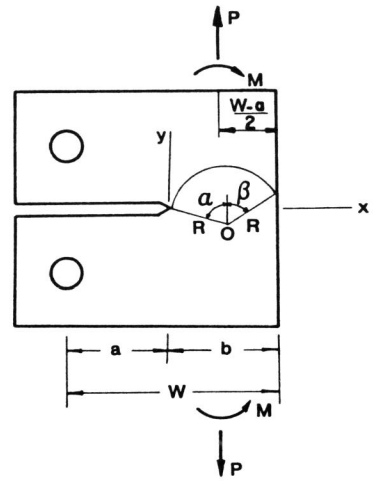


Fig. 2. Circular Slip Line

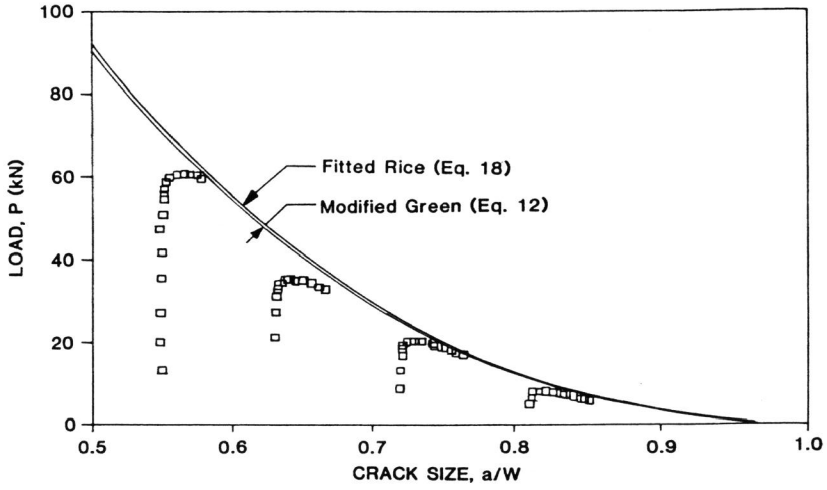


Fig. 3. Crack Extension in 1T-C(T) Specimens of A533B Steel with Different Initial Crack Extension

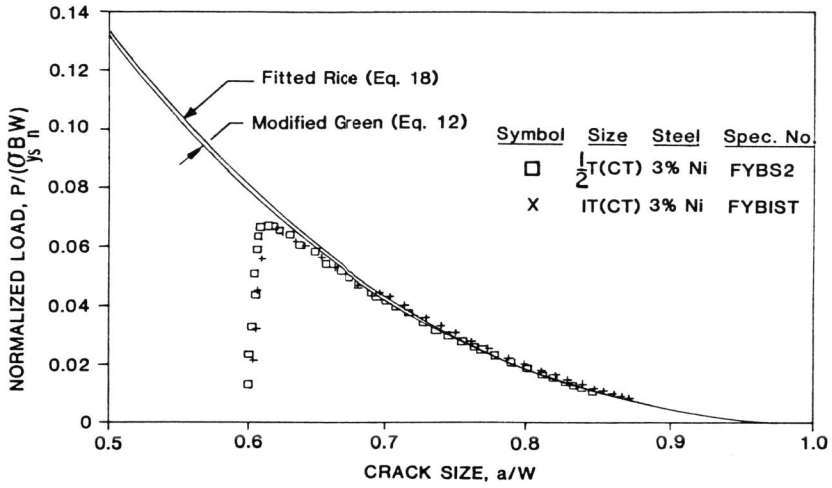


Fig. 4. Crack Extension in C(T) Specimens of 3% Ni Steel of Different Specimen Size

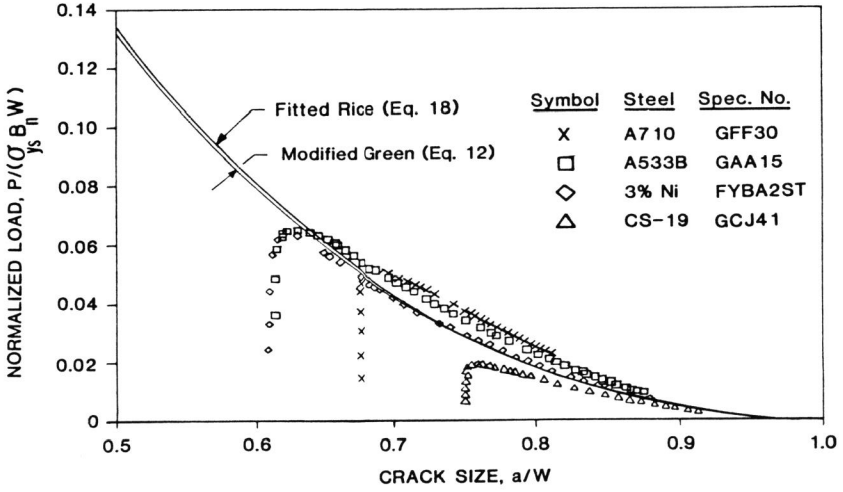


Fig. 5. Crack Extension in 1T(CT) Specimens of Different Metals